High Energy Density Physics 52 (2024) 101122

Contents lists available at ScienceDirect

High Energy Density Physics

journal homepage: www.elsevier.com/locate/hedp

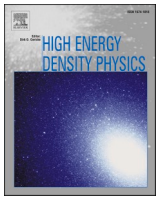

Physical properties of rutile-TiO_2 Nanoparticles and effect on PVA/SiO_2 hybrid films synthesized by sol-gel method

B. Gueridi [a], K. Bouferrache [b], M.A. Ghebouli [c,d], F. Rouabah [a], Y. Slimani [e], T. Chihi [c], M. Fatmi [c,*], B. Ghebouli [f], H. Bouandas [c], M. Habila [g], A. Benali [h]

[a] Laboratory of Physico-chemistry of High Polymers (LPCHP), Department of Process Engineering, Faculty of Technology, Ferhat Abbas University - Setif-1-, Setif, 19000, Algeria
[b] Department of Physics, Faculty of Sciences, University of Mohamed Boudiaf, M'sila, 28000, Algeria
[c] Research Unit on Emerging Materials (RUEM), University Ferhat Abbas of Setif 1, Setif, 19000, Algeria
[d] Department of Chemistry, Faculty of Sciences, University of Mohamed Boudiaf, M'sila, 28000, Algeria
[e] Laboratory of Intelligent System (LSI), Faculty of Technology, University Ferhat Abbas of Setif 1, Setif, 19000, Algeria
[f] Laboratory for the Study of Surfaces and Interfaces of Solid Materials (LESIMS), University Ferhat Abbas of Setif 1, Setif, 19000, Algeria
[g] Department of Chemistry, College of Science, King Saud University, P.O. Box 2455, Riyadh, 11451, Saudi Arabia
[h] 4I3N and Physics Department, University of Aveiro, 3810-193, Aveiro, Portugal

ARTICLE INFO

Keywords:
Thermoelectric properties
TiO_2
Thermal conductivity
Sol gel

ABSTRACT

We use an *ab-initio* approach to analyze the structural, electronic band structure, and thermoelectric properties of titanium dioxide (TiO_2 in rutile phase), and we then use rutile-TiO_2 nanoparticles to determine its effects on sol-gel-produced polyvinyl alcohol/silicon dioxide (PVA/SiO_2) hybrid films. The synthesis of hybrid films involved the incorporation of 1 % rutile-TiO_2 nanoparticles in the PVA/SiO_2 matrix. The thermoelectric properties of the resulting hybrid films were characterized by Seebeck coefficient measurements, as well as electrical and thermal conductivities. The synthesis of PVA/SiO_2/Nano-TiO_2 films was accomplished with success. The chemical bonds have amply demonstrated that the PVA backbone is connected to the (SiO_2-TiO_2) network. TGA testing indicates that hybrid films are more resistant to higher temperatures than pure PVA films. SiO_2 nanoparticles reveal more effective loading to improve dielectric characteristics compared to TiO_2. The best results are obtained in cases of mechanical, thermal and electrical insulation when both nanofillers are integrated into the polymer matrix. The findings show that the thermoelectric performance of PVA/SiO2 hybrid films is improved by the addition of (1 %) rutile-TiO_2 nanoparticles in the rutile phase. This study provides insights into the potential applications of rutile-TiO_2 nanoparticles in enhancing the thermoelectric properties of hybrid materials and opens up avenues for further research in this area, and contributes to the growing body of knowledge on enhancing the thermoelectric properties of materials by incorporating rutile-TiO_2 nanoparticles into hybrid films synthesized by the sol-gel method.

1. Introduction

Several researchers have intensively studied the physical and chemical properties of titanium dioxide TiO_2 and explored more applications in various fields. The rutile structure of TiO_2 material is the most important. Its structure, electronic and optical properties have been studied experimentally by different methods, and theoretically by functional theory approaches (DFT). In recent years, research has focused on developing thermoelectric materials, with enhanced performance by incorporating nanomaterials into traditional thermoelectric materials, due to their ability to convert waste heat into useful electrical energy. One such nanomaterial is titanium dioxide (rutile-TiO_2) nanoparticles, which have shown promising results in enhancing the thermoelectric properties of various materials. Titanium dioxide rutile-TiO_2 nanoparticles [1] is a natural transition metal oxide. Titanium dioxide is a semiconductor that is more efficient than other materials and has better stability [2–6]. Titanium dioxide has many applications as a synthesis of organic compounds [7–10]. Studies have devoted to the synthesis of various forms of nanomaterials [11–13], designed with doping [14–17] or composites [18–20]. TiO_2 exists naturally in three

* Corresponding author.
E-mail address: fatmimessaoud@yahoo.fr (M. Fatmi).

https://doi.org/10.1016/j.hedp.2024.101122
Received 24 August 2023; Received in revised form 15 May 2024; Accepted 10 June 2024
Available online 11 June 2024

crystalline forms, rutile (tetragonal, space group $P4_2/mnm$), anatase (tetragonal, space group $I4_1/amd$), brookite (orthorhombic, space group Pbca) [21–24]. In addition, there is another polymorph TiO_2 (B) (monoclinic, space group C2/m), whose rutile is the most thermodynamically 1.88 eV [25–27]. Acetic acid was used to create anatase nanoparticles, whereas hydrochloric acid with different dosage was used to create rutile and brookite nanoparticles. Using the dip coating process followed by aging treatment to fabricate PVA/SiO_2-TiO_2 hybrid fibers from the hybrid sols. M. Haihong et al. [28], characterized the system by SEM (scanning electron microscope) measurements and showed that the system was homogeneous and that the fibers have a diameter of approximately 50 nm when they reach their maximum spinning length. According to thermogravimetric analysis (TG) studies, hybrid fibers exhibit greater heat resistance than pure PVA fibers. The sol-gel method has emerged as a popular technique for synthesizing hybrid materials, particularly PVA/SiO_2 hybrid films, due to its simplicity, low cost, and versatility. The incorporation of rutile-TiO_2 nanoparticles into PVA/-SiO_2 hybrid films synthesized via the sol-gel method has the potential to enhance their thermoelectric properties.

We organize the article such that the detail of the ab initio calculations provided in a large section I. The experimentally calculated results and discuss them in a large section. In this part; the study aims to investigate the effect of rutile-TiO_2 nanoparticles on the thermoelectric properties of PVA/SiO_2 hybrid films synthesized by the sol-gel method. The thermoelectric properties, including the Seebeck coefficient, electrical and thermal conductivities, will be characterized and analyzed to determine the optimal concentration of rutile-TiO_2 nanoparticles in the hybrid films. Previous studies have shown that rutile-TiO_2 nanoparticles improve the thermoelectric properties of materials, including polymers and inorganic materials. For example, rutile-TiO_2 nanoparticles incorporated into poly (3-hexylthiophene) (P3HT) improve its thermoelectric performance [29]. Likewise, a synthesized TiO_2/polyimide composite film was studied in order to enhance the thermoelectric properties. Furthermore, the sol-gel method has been widely used for synthesizing hybrid materials, including PVA/SiO_2 hybrid films, due to its simplicity and versatility [30–32]. Improving the thermoelectric properties of hybrid materials proves useful and crucial by incorporation of TiO_2 nanoparticles into hybrid films synthesized by the sol-gel method [30].

2. Experimental

2.1. Materials

The following materials were provided by Sigma-Aldrich: Tetraethyl orthosilicate (TEOS) (98%, Mw = 208.33 g/mol, d = 0.933 g/ml); hydrochloric acid (HCl) (38 %, M = 36.46 g/mol, d = 1.19 g/ml); ethanol (C_2H_5OH) (96 % (v/v) Mw = 46.07 g/mold = 0.789 g/ml); poly (vinyl alcohol) degree of polymerization= 1800, 98 % hydrolyzed with Mw= 15,000, and TiO_2 in rutile phase with an average particle size of 10–25 nm. All of the trials utilized deionized water (DI). Without any additional purification, all chemicals and supplies were procured and used exactly as received. To explore the physical and thermal properties, DSC and TGA techniques were used.

2.2. Preparation of films

The preparation of films used in this investigation is described in this section. The PVA film was created by dissolving 5 g of PVA using magnetic mixing in 100 ml of deionized water (5 %) and heating the resulting liquid to 80 °C for an hour to get a homogeneous and viscous consistency. The gel was finally moved to a petri dish and left to solidify for three days at room temperature. TEOS was dissolved in ethanol, deionized water, and HCl at a molar ratio of 1:4:1:0.04 to create the PVA/SiO_2 film in the same manner as the clean PVA film. The TEOS solution was combined with a small amount of PVA solution, and the combination was then agitated for an hour at 60 °C. Following that, the fluid was left to rest for three days at room temperature in an incubator. To make the PVA/SiO_2/TiO_2 film, rutile-TiO_2 nanoparticles were introduced to water and magnetically spun for three hours. After that, sonication was used for an hour in order to stop the nanoparticles from aggregating. The PVA/SiO2 solution was prepared as previously described, and then the mixture of rutile-TiO_2 nanoparticles was added and mixed under magnetic stirring for an hour before being sonicated for one hour. The liquid was poured onto a Petri dish and left to solidify at room temperature for three days. Table 1 summarizes the composition of the hybrid films.

3. Results and discussion

3.1. Structural properties

We studied the structural behavior of rutile-TiO_2 nanoparticles in $P4_2/mnm$ (N°136) phase using GGA approximation. The atomic positions of Ti and O are (1/2,1/2,0), (0.6956,0.6956,1/2) respectively. The WIEN2k code [33,34] fixes all parameters. The initial Brillouin zone has 1000 k-points, and the cutoff parameter was set at $R_{MT}.K_{max}$= 9, where K_{max} is the largest value of the reciprocal lattice vector of the plane wave expansion and R_{MT} is the smallest atomic sphere radius in the unit cell. Table 2 shows the values of $R_{MT}.K_{max}$, R_{MT} (Ti), R_{MT} (O) and k-points of TiO_2 using Generalized Gradient Approximation (GGA). A better optimization was obtained by changing K-points and $R_{MT}.K_{MAX}$. The lattice parameters corresponding to k-point 3000 and $R_{MT}.K_{MAX}$ of 9 are consistent with the experimental values.

The lattice parameters, bulk modulus, and its pressure derivative are determined using the GGA technique. The crystal structure of the P42/mnm phase of rutile-TiO2 nanoparticles was visualized in Fig. 1. The minimum cohesive energy which ensures the compounds stability in the tetragonal phase under the effect of the volume of TiO_2 at atmospheric pressure is shown in Fig. 2.

3.2. Band structure and density of states

The computed band structure of rutile-TiO_2 nanoparticles and associated density of states (DOS) are shown in Figs. 3–5. For rutile TiO_2 nanoparticles the electronic structure was calculated using GGA (PBE). In the Brillouin zone, we notice that rutile TiO_2 nanoparticles have a straight gap of 1.954 eV, which agree with the values reported in literature 1.78 eV [34] and 1.88 eV [35]). The vertical solid line at 0 eV in these graphs represents the Fermi level. However, when examining the partial and total DOSs, it is difficult to see the band crossing. Thus, as illustrated in Fig. 4, the DOS can be zoomed very nearly to the Fermi level. DOSs cross the Fermi level, as demonstrated by the zoomed figures. This is once more congruent with our findings about the band organization and entirely consistent with P.R. Varadwaj et *al.* [36].

The electronic states close to the Fermi level are denser, which is significant to the materials' excellent thermoelectric properties. We talk about the Fermi energy electronic structure because thermoelectric qualities depend on it, because the state density is so near to the Fermi level, the 3*d*-Ti and 2*p*-O states contribute significantly to the valence band edge, which has a significant impact on the thermoelectric performance of the materials. O-2*p* states and Ti-3*d* states, respectively, make up the valence band's (VB) top and conduction band's (CB) bottom. We observe some mingling of the O-2*p* states with the Ti-*d* states. Furthermore, Ti-*s* PDOS in the valence band region had a clearly smaller width than O-*s* did. We provide the partial density of states for each atom in rutile-TiO_2 nanoparticles in Fig. 5, using the GGA functional.

3.3. Thermoelectric properties (Seebeck coefficient (SC))

The SC is the most crucial factor in determining how a material reacts to a temperature differential. In order to enhance a material's thermoelectric nature for practical manifestation, the amount of doping or the

Table 1
Compositions and preparation of PVA/SiO_2/TiO_2 hybrid solutions. P: Neat PVA, PS:PVA/SiO2, PST: PVA/SiO2/TiO2 (1wt%).

Sample	PVA (Wt%)	TEOS (Wt%)	Silica (W%)	TEOS (wt%) in Solution	PVA (wt%) in the solution	silica: PVA ratio in solution	H2O/TEOS (mol) ratio	HCL/TEOS (mol) ratio	TiO2 (g)	Appearance of the films
P	100	0	0	0	5	0:1	0	0	0	Transparent
PS	60	40	16	3	4.5	1:1.5	1	0.04	0	Transparent
PST	60	40	16	3	4.5	1:1.5	1	0.04	0.5	opaque white

Table 2
Values of $R_{MT}.K_{max}$, k-point, lattice parameters, volume, bulk modulus, pressure derivative of bulk modulus and minimum energy of rutile-TiO_2 nanoparticles (136_$P4_2$/mnm) using GGA.

$R_{MT}.K_{MAX}$	K-point	a	b	c	V_0	B	B'	E_0
9	1000	4651(4.60 [34])	4651(4.60[34])	2828(2.96[34])	433,563	228,411	2151	-4018,0683
	2000	4.650	4.650	2.965	432.733	225.49	3.984	-4018.096
	3000	4.610	4.610	2.965	431.633	225.50	3.992	-4018.096
	4000	4.648	4.648	2.964	432.263	226.30	4.451	-4018.09
9,5	1000	4642	4642	2823	433.563	228.466	2.148	-4018.068
	2000	4.373	4.373	3.348	432.286	226.232	4.315	-4018.130
	3000	4.648	4.648	2.964	432.278	226.278	4.398	-4018.092
	4000	4.373	4.373	3.348	432.274	226.138	4.402	-4018.496

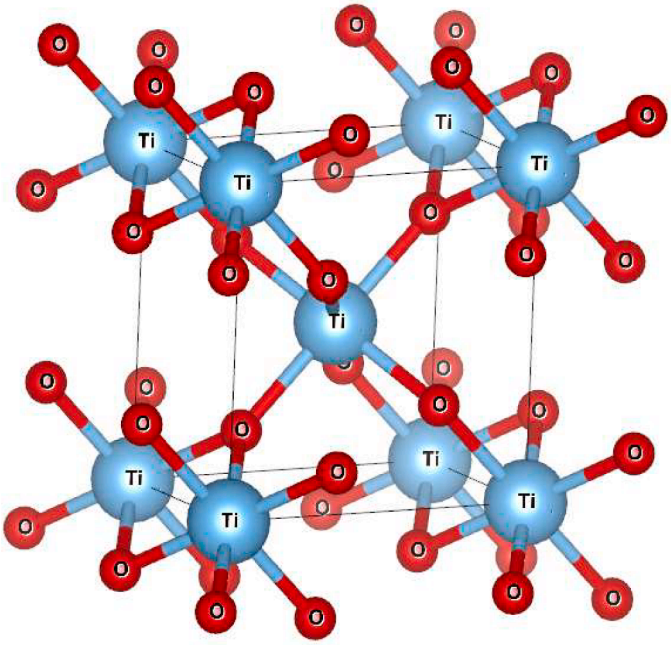

Fig. 1. Rutile-TiO_2 nanoparticles structure in $P4_2$/mnm.

concentration of carriers in the material are determined by the chemical potential. The magnitude of the charge carrier concentration that corresponds to the chemical potential is, however, determined by the actual electrical band structure. The SC of rutile-TiO_2 nanoparticles is plotted against the chemical potential at 300 K, 600 K and 800 K as shown in Fig. 6(a). In the *p*- and *n*-type areas, the SC values for the examined chemical are symmetric and near to the Fermi level. It is now understood that the contribution of the holes in the *p*-type region of rutile-TiO_2 nanoparticles is proportional to that in the *n*-type region. The *n*-type zone's high SC values show that *n*-type doping predominates over *p*-type doping in these types of materials, even if the *p*-type region has identical characteristics of SC values and the chemical favors strong doping. The computed Seebeck coefficient's maximum values in the *n*-type area for 300, 600, and 800 K are 2892, 1592, and 1212 V/K, respectively, denoting= 0.7, 1, and 1. For the same temperatures in the *p*-type area, 2826, 1410, and 1047 V/K were observed in Fig. 6.

3.4. Electrical conductivity

In metals, electrons dominate the electrical conductivity, whereas in semiconductors, electrons and holes contribute to electrical conductivity. Good conductors have large free carriers which are used in thermoelectric materials. In the context of the materials' ordered electrical conductivity, we have estimated the electronic structure of the rutile-TiO_2 nanoparticles compound. In Fig. 6, electrical conductivity per relaxation time for materials made of rutile-TiO_2 nanoparticles are plotted versus chemical potential, where chemical potential stands in for doping or the concentration of charge carriers. In spite of the fact that both *p*-type and *n*-type regions with high doping levels have high values, the figure clearly demonstrates that *p*-type regions have higher valence band carrier concentrations than *n*-type regions. At 300 K, the highest rutile-TiO_2 nanoparticles value in the *p*-type region is 3.82 10^{20} (ms), and rutile-TiO_2 nanoparticles values decrease with increasing temperature.

3.5. Electronic thermal conductivity

It is possible to compute the overall thermal conductivity of a material (k) by adding the thermal conductivities of phonons and conduction electrons, or ke and kl, respectively. In a semiconductor, phonons predominate the thermal conductivity; whereas, in metals, this contribution is primarily made by electrons or free carriers [37–39]. For temperatures of 300 K, 600 K, and 800 K, Fig. 6 illustrates the relationship between chemical potential and electronic thermal conductivity per relaxation time. In the *n*-region or the *p*-region, k- rises with rising temperature for a constant chemical potential. With a peak value of around 2.38 10^{14}W/mKs for 300 K, 5 10^{14}W/mKs for 600 K, and 6.5 10^{14} W/mKs for 800 K, rutile-TiO_2 nanoparticles exhibits a greater increase in k/τ in this situation. The k/τ response for the n-type is non-significant when compared to the p-type region. The greatest values in the n-type region are 2.5 10^{14}W/mKs, 4.5 10^{14}W/mKs, and 5.5 10^{14}W/mKs for 300 K, 60 K, and 800 K, respectively.

3.6. Power factor (PF)

In comparison to the SC and electrical conductivity, the (PF) is the most thorough parameter to analyze a material's thermoelectric performance. It can be expressed mathematically as PF= S^2, where S stands for the SC and C for a particular material's electrical conductivity. Fig. 6 (e) depicts the chemical potential dependency of the PF for rutile-TiO_2 nanoparticles. The PF was measured in 10^{10}W/cmK^2s units. The

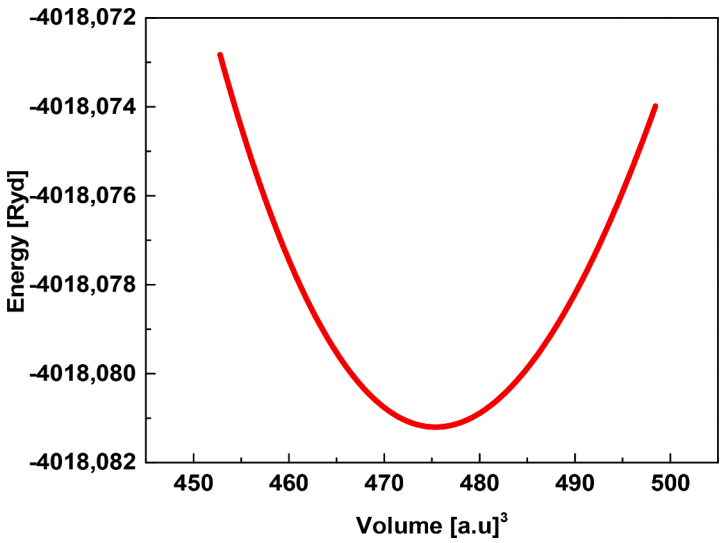

Fig. 2. The variation of the cohesive energy as a function of unit cell volume for rutile-TiO_2 nanoparticles in $P4_2/mnm$ structure.

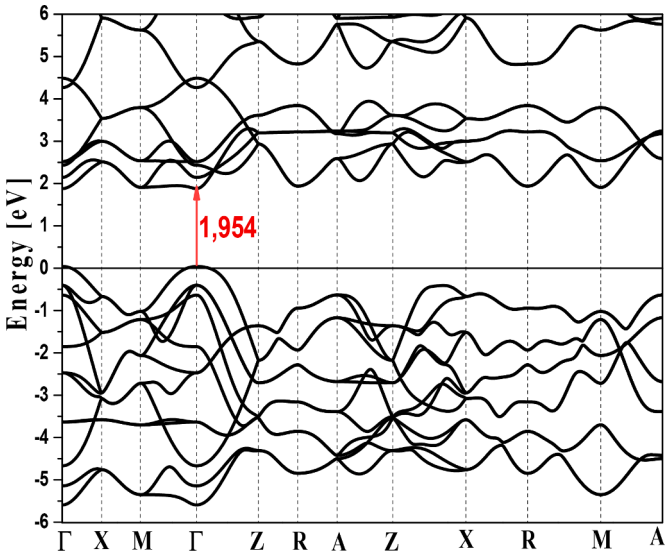

Fig. 3. Electronic band structures of rutile-TiO_2 nanoparticles in$P4_2/mnm$ using GGA.

chemical potential range between [1.5 eV, 2.5 eV] is where the PF is at its highest. As a result, the latter range might be viewed as a crucial area for rutile-TiO_2 nanoparticles excellent performance. In all the materials being studied, the PF for the chemical potential for the p-type area is close to -0.5eV For 300 K, 600 K, and 800 K, the increase and decline are strongest for 300 K. Until the chemical potential reaches a value of -0.5 eV, this PF number is still small. The n-type region has greater PF values than the p-type region, indicating that n-type doping predominates over p-type doping at all temperatures. The n-type region is obtained with similar PF values, and the compound favors low doping. The computed PF_{max} for rutile-TiO_2 nanoparticles at its highest value in the n-type region is 175 10^{10} W/cmK^2s for 800 K, 130 10^{10} W/cmK^2s for 600 K and 50 10^{10} W/cmK^2s for 300 K, i.e. when the temperature increases the PF_{max} increases at μ= 2 eV After falling as, the chemical potential increased, the PF value in the n-type area becomes negligible at a chemical potential of 3 eV It is evident that the computed PF rapidly rises with rising temperature; in addition, PF rises more quickly in n-type than p-type.

3.7. Thermal properties

DTA measures weight changes as a function of temperature. The measured weight loss curve provides information on changes in sample composition and its thermal stability. The thermogravimetric thermograms of composites PVA, PVA/SiO_2 and VA/SiO_2/TiO_2 samples are shown in Fig. 7 (a, b).

The thermal degradation of Pure PVA exhibits three significant weight loss zones, as shown in Fig. 7a [40]. The small initial area occurs between 224 and 486 °C, with T_{max}, step1= 95 °C being the temperature at which the most weight is lost. This results from both free-floating and bound water molecules evaporating. A modest (20 %) weight loss is visible at this time. The elimination of leftover solvent molecules is the cause of this weight loss [41]. The second zone, with the highest rate of decomposition, is found between 224 and 486 °C. The estimated 15 % weight loss is due to the degradation of the (-OH) side group, which leads to the formation of a polygene at a step 2 temperature of 270 °C. It is possible to connect the third step, which is seen in the range of 410 to 450 °C with (T_{max},) step3= 430 °C, to the dissolution of the PVA polymer's main chain (cleavage of the C—C backbone), which is currently known as carbonation or so-called carbonation. The penultimate phase at 600 °C causes a weight loss of 91 %, leaving a final residue of 9 %. After silica was added to the PVA matrix, the PVA/SiO_2 membranes' thermal stability improved. In this example, the PVA/SiO_2 thermogram exhibits four weight-loss zones that decrease gradually [42]. The hydrogen interaction between PVA chains and the silanol ends of the silica may be what causes the breakdown of the crystalline structure and the change to a more amorphous state. The DSC sections have already covered and emphasized this explanation. The initial weight loss is projected to be 6 %. This is because, at (T = 30, 170 °C) [43], silanol groups participate in the self-condensation reaction that occurs after the last solvent molecule is removed. The remaining temperature ranges where weight loss took place were 170 to 390 °C, 390 to 490 °C, and 490 to 690 °C. The temperatures of 120, 330, 455, and 590 °C, result in the largest weight loss. The hydroxyl groups are breaking down with other organic PVA and silica network residues at high temperatures. The ultimate residual weight has a residue of 20% overall and ranges from 76.9% to 83.6 % of the total weight. It is expected that including a silica network into the PVA matrix polymer will improve the films' thermal stability. Fig. 7b depicts the TGA curves for PVA/SiO_2 with 1 % rutile-TiO_2 nanoparticles content. After being integrated with the silica network, tidy PVA's enhanced heat tolerance was apparent. The TGA thermograms of PVA/SiO_2/TiO_2(1 %) exhibit a similar behavior to that of PVA/SiO_2 hybrid films with regard to heat deterioration. The quantity

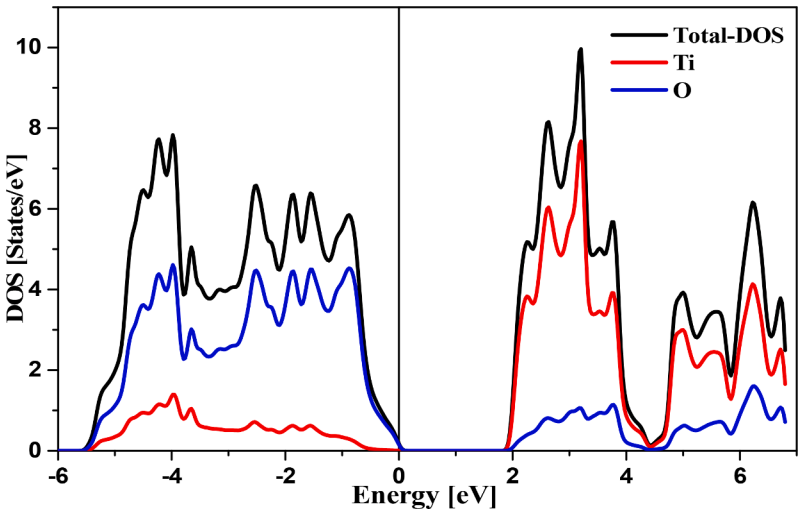

Fig. 4. The density of states for rutile-TiO_2 nanoparticles in $P4_2/mnm$ computed by GGA.

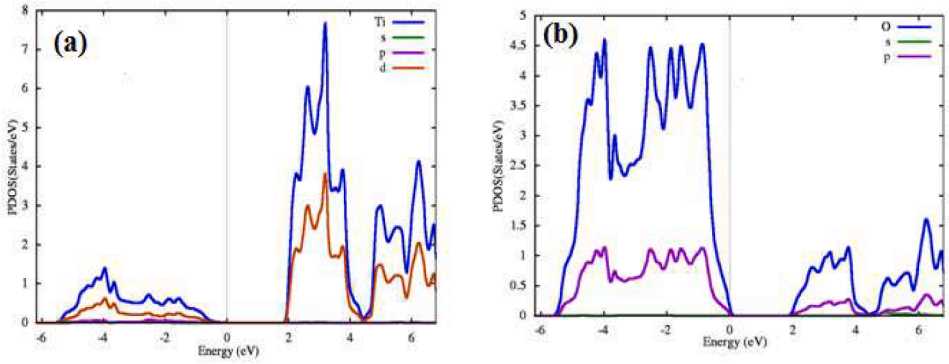

Fig. 5. The partial density of states for Ti (a) and O atoms (b) using GGA functional.

of final residual weight distinguishes the four main weight loss areas observed on the thermograms. At a temperature of 700 °C, the sample PVA/SiO_2/TiO_2 (1 %), has a final residual weight of 17.84 % in relation to the global weight. This suggests that adding 1 % rutile-TiO_2 nanoparticles to PVA/SiO_2 improves its thermal stability. PVA/SiO_2 nanocomposite films were strengthened with rutile-TiO_2 nanoparticles to improve their thermal stability. The temperatures (Tc, Tm) for crystallization and melting in this study were measured using DSC measurements. The four main weight loss zones visible on the thermograms can be distinguished based on the final residual weight amount is shown in Figs. 8 (a-c). The curves represent both exothermic and endothermic reactions. PVA/SiO_2 exhibits a melting endothermic peak with a drop of 26 °C that is broader, less abrupt, exceedingly weak, and broad than PVA neat. At 193 °C, which is the melting temperature, PVA shows a comparatively big and steep melting endothermic peak as shown in Fig. 8b. The crystallization area (Tc), which is an exothermic peak that is seen for Neat PVA at a temperature of 112 °C, is not present for PVA/-SiO_2. Other works [44] also found similar discoveries. For instance, Y. Bin et *al.* [45] demonstrated this type of behavior in PVA-MWNT and PVA-VGCF composites. The PVA segments' endothermic peak gradually diminished and disappeared for all samples. These results differ from what is commonly reported in the literature [46]. The broadening of the peak and decrease in melting temperature show that the inclusion of silica and TiO_2 nanoparticles changed the regular structure of PVA molecules. The thermoelectric properties of the generated hybrid films were evaluated using tests for thermal and electrical conductivities. To better comprehend the phenomena of the rutile-TiO_2 nanoparticles, which is used in the sol-gel method of synthesis of PVA/SiO_2 hybrid films and boosts the thermoelectric properties, an ab-initio investigation is necessary.

4. Conclusions

At various chemical potentials of rutile-TiO_2 nanoparticles, we investigated the effects of functional on the structural, electronic band structures, and thermoelectric characteristics. The outcome suggests that chemical potential has a significant impact on these compounds' thermoelectric properties. This research sought to determine how the addition of rutile-TiO_2 nanoparticles affected the thermoelectric characteristics of sol-gel-produced PVA/SiO_2 hybrid films. The study's findings demonstrated that adding rutile-TiO_2 nanoparticles, at the right concentration, considerably improved the PVA/SiO_2 hybrid films' thermoelectric performance. The unique characteristics of rutile-TiO_2 nanoparticles, such as their high electrical conductivity and low heat conductivity, are responsible for the improved thermoelectric performance. These characteristics result in an improvement in the thermoelectric performance by increasing the Seebeck coefficient and electrical conductivity, while decreasing the thermal conductivity. This study contributes to the growing body of knowledge on enhancing the thermoelectric properties of materials by incorporating rutile-TiO_2 nanoparticles into hybrid films synthesized by the sol-gel method. The results of this study can potentially pave the way for the development of high-performance thermoelectric materials for various applications, including power generation and refrigeration. Further research can focus on investigating the influence of other factors, such as the size and shape of rutile-TiO_2 nanoparticles, on the thermoelectric properties of

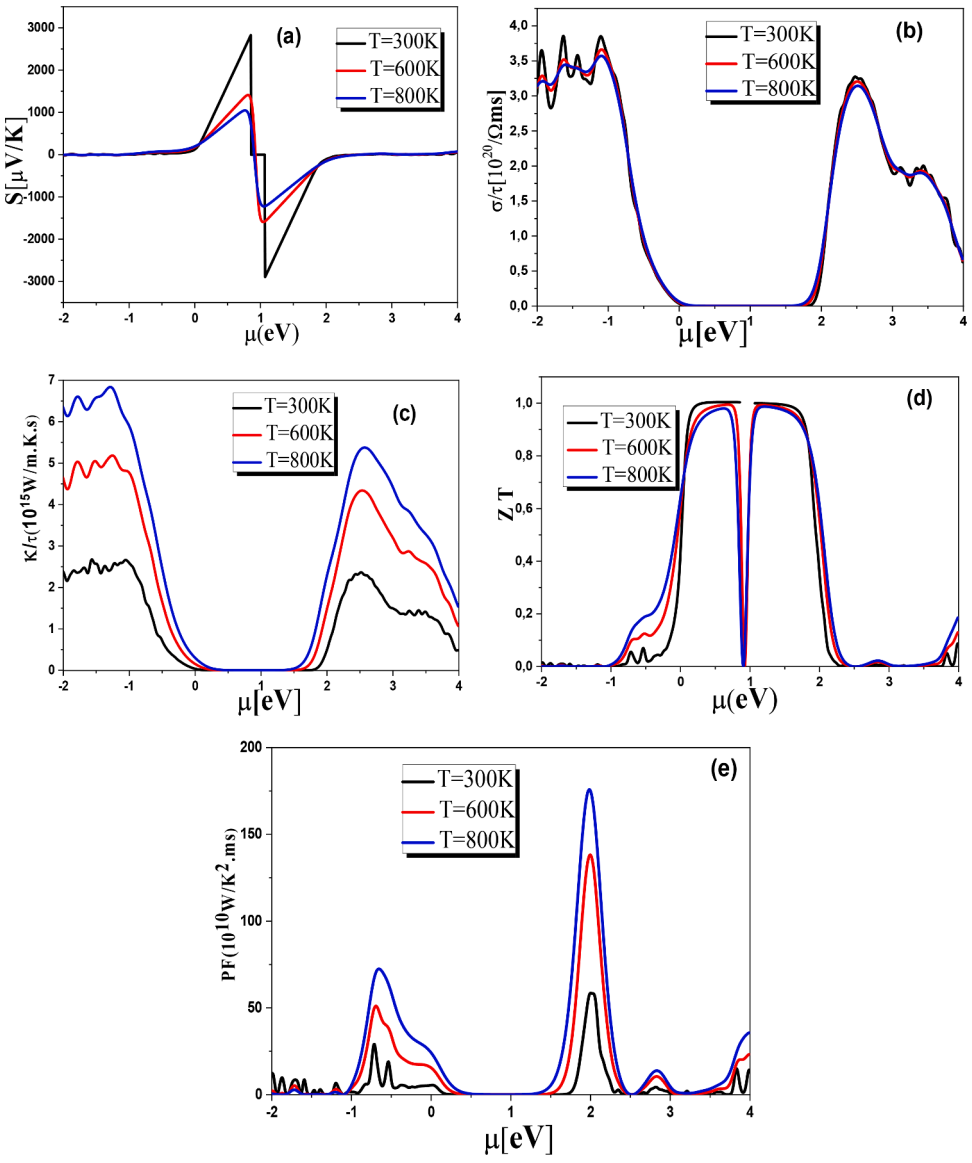

Fig. 6. The Seebeck coefficient (a), electrical conductivity (b), electronic thermal conductivity (c), figure of merit (d), and power factor (e) for rutile-TiO_2 nanoparticles $P4_2/mnm$ at T= 300 K, 600 K, and 800 K.

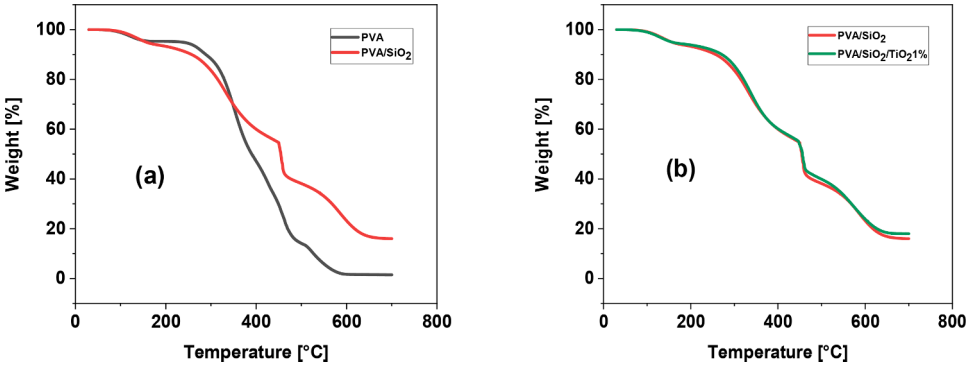

Fig. 7. TGA thermograms of Pure PVA, PVA/SiO_2 (a) and PVA/SiO_2 films with 1 % (b) of rutile-TiO_2 nanoparticles.

hybrid films. Additionally, the development of hybrid materials with enhanced thermoelectric performance can be explored by incorporating other nanomaterials into the PVA/SiO_2 matrix. Overall, this study provides insights into the potential applications of rutile-TiO_2 nanoparticles in enhancing the thermoelectric properties of hybrid materials and opens up avenues for further research in this area.

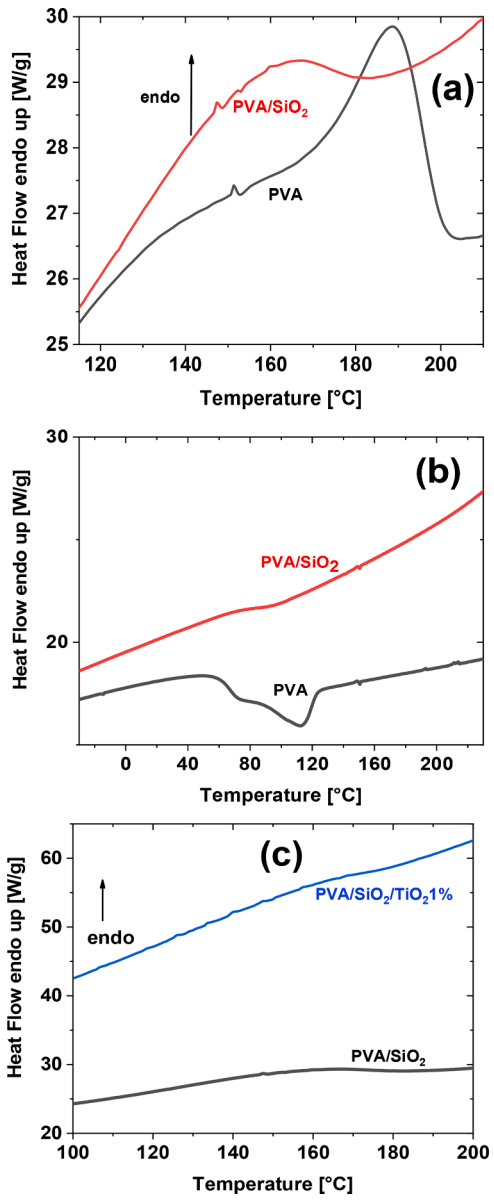

Fig. 8. DSC curves of melting peaks PVA and PVA/SiO_2, (a) crystallization peaks PVA and PVA/SiO_2, melting peaks for PVA/SiO_2 (b), and PVA/SiO_2films with rutile-TiO_2 nanoparticles content of 1 % (c).

CRediT authorship contribution statement

B. Gueridi: Investigation, Funding acquisition. **K. Bouferrache:** Methodology. **M.A. Ghebouli:** Writing – original draft. **F. Rouabah:** Project administration. **Y. Slimani:** Project administration. **T. Chihi:** Resources. **M. Fatmi:** Writing – original draft, Visualization, Validation. **B. Ghebouli:** Writing – original draft. **H. Bouandas:** Formal analysis. **M. Habila:** Supervision, Software. **A. Benali:** Methodology.

Declaration of competing interest

The author(s) declared no potential conflicts of interest with respect to the research, authorship, and/or publication of this article.

Data availability

The data that has been used is confidential.

Acknowledgements

This work was funded by the Researchers Supporting Project Number (RSP2024R441), King Saud University, Riyadh, Saudi Arabia.

References

[1] A.J. Haider, Z.N. Jameel, I.H. Al-Hussaini, Procedia 157 (2019) 17–29.
[2] D.R. Eddy, S.N. Ishmah, M.D. Permana, M.L. Firdaus, Catalysts 10 (2020) 1248.
[3] X. Chen, S.S. Mao, Chem. Rev. 1072891 (2007) 2959.
[4] K.M. Glassford, J.R. Chelikowsky, Phys. Rev. B 46 (1992) 1284–1298.
[5] F.A. Grant, Rev. Mod. Phys. 31 (1959) 646–674.
[6] R.G. Breckenridge, W.R. Hosler, Phys. Rev. 91 (1953) 793–802.
[7] Z. Lin, Y. Zheng, F. Deng, X. Luo, J. Zou, P. Shao, S. Zhang, H. Tan, Purif. Technol. 277 (2021) 119430.
[8] J.S. Hubbard, J.P. Hardy, G.E. Voecks, E.E. Golub, J. Mol. E 2 (1973) 149–166.
[9] M.J. Lima, A.M. Silva, C.G. Silva, J.L. Faria, N.M. Reis, Chem. Eng J 430 (2022) 132643.
[10] J. Luo, M. Wang, L. Chen, J. Shi, J. Energy Chem. 66 (2022) 52–60.
[11] J. Chen, F. Qiu, W. Xu, S. Cao, H. Zhu, Appl. Catal. A Gen 495 (2015) 131–140.
[12] P. Dong, G. Hou, X. Xi, R. Shao, F. Dong, Environ. Sci. Nano 4 (2017) 539–557.
[13] Y. Zhong, J. Wang, R. Zhang, W. Wei, H. Wang, X. Lü, F. Bai, H. Wu, R. Haddad, H. Fan, Nano Lett. 14 (2014) 7175–7179.
[14] X. Li, W. Zheng, G. He, R. Zhao, D. Liu, ACS. Sustain. Chem. Eng. 2 (2014) 288–295.
[15] M.A. Rauf, M.A. Meetani, S. Hisaindee, Desalination 276 (2011) 13–27.
[16] V. Kumaravel, S. Mathew, J. Bartlett, S.C. Pillai, Appl. Catal. B 244 (2019) 1021–1064.
[17] Y.C. Nah, I. Paramasivamand, P. Schmuki, Chem. Phys. Chem. 11 (2010) 2698–2713.
[18] K. Woan, G. Pyrgiotakis, W. Sigmund, Adv. Mater. 21 (2009) 2233–2239.
[19] B. Tang, H. Chen, H. Peng, Z. Wang, W. Huang, Nanomater. 8 (2018) 105.
[20] J. He, A. Kumar, M. Khan, I.M. Lo, Sci. Total Environ. 758 (2021) 143953.
[21] D. Tekin, D. Birhan, H. Kiziltas, Mat. Chem. Phys. 251 (2020) 123067.
[22] E. Murad, Am. Mineral 82 (1997) 203–206.
[23] Y. Lu, B. Jaeckel, B.A. Parkinson, Langmuir 22 (2006) 4472–4475.
[24] J.E. Haggerty, L.T. Schelhas, D.A. Kitchaev, J.S. Mangum, L.M. Garten, W. Sun, Sci. Rep. 7 (2017) 15232.
[25] M.D. Permana, A.R. Noviyanti, P.R. Lestari, N. Kumada, D.R. Eddy, I. Rahayu Kuwait, J. Sci. 49 (2022) 1–13.
[26] G. Deo, A.M. Turek, I.E. Wachs, T. Machej, J. Haber, N. Das, H. Eckert, A.M. Hirt, Appl. Catal. A Gen. 91 (1992) 27–42.
[27] D. Reyes-Coronado, G. Rodrıguez-Gattorno, M.E. Espinosa-Pesqueira, C. Cab, R. de Coss, G. Oskam, Nanotechnology 19 (2008) 145605.
[28] M. Haihong, S. Tiejun, S. Qiusheng, Fibers 2 (2014) 275–284.
[29] J. Kim, S. Lim, S. Cha, H.S. Kim, S.H. Kim, H. Lee, Synth. Metals 217 (2016) 171–176.
[30] L. Zhang, Y. Zhang, X. Gao, S. Han, Q. Yu, J Mater. Sci. Mater. Electron. 13 (2020) 10836–10845.
[31] Y. Lu, M. Zhang, Y. Chen, X. Chen, C. Zhou, W. Huang, J. Sol-Gel Sci. Technol. 91 (2) (2019) 437–445.
[32] H. Zhang, B. Li, X. Li, Q. Li, J. Zhang, H. Lu, J. Sol-Gel Sci. Technol. 66 (3) (2013) 392–399.
[33] P. Blaha, K. Schwarz, G. Madsen, D. Kvasnicka, J. Luitz, WIEN2k, an augmented plane wave plus local orbitals program for calculating crystal properties user's guide, WIEN2k Austria: vienna University of Technology, Inst. Phys. Theor. Chem. Getreidemarkt 142 (2014).
[34] T.A. Al-DhahirP, K. Blaha, G. Schwarz, D. Madsen, J. Kvasnicka, Luitz WIEN2k, an augmented plane wave plus local orbitals program for calculating crystal properties user's guide, WIEN2k 142, Austria: vienna University I Alaitham, Diyala J. Pur Sci. 9 (2013) 108–119.
[35] M. Landmann, E. Raulsand, W.G. Schmidt, J. Condens, Matter Phys. 24 (2012) 195503.
[36] P.R. Varadwaj, V.A. Dinh, Y. Morikawa, R. Asahi, ACS Omega 24 (2023) 22003–22017.
[37] C. Kittel, Introduction to Solid State Physics USA, eighth ed, John Wiley & Sons, Hoboken, 2004, p. 156.
[38] M. Bilal, I. Ahmad, S.J. Asadabadi, R. Ahmad, M. Maqbool, Electron. Mater. Lett. 11 (3) (2015) 466–480.
[39] T.M. Tritt, Thermal Conductivity: Theory, Properties, and Applications USA, Kluwer Academic/PLENUM publishers, New York, 2004, p. 75.
[40] C.C. Yang, J. Membr. Sci. 288 (2007) 51–60.
[41] N.A. Betti, Eng. Tech. J. 34 (2016) 2433–2442.
[42] F. Quan, L.L. Chen, Y. Xiaand, Q. Ji, Polym. Polym. Compos. 17 (2009) 97–100.
[43] H. Awadaand, C. Daneualt, Appl. Sci. 5 (2015) 840–850.
[44] J.M. Dodda, P. Bělský, J. Chmelař, T. Remiš, K. Smolná, M. Tomáš, L. Kullováand, J. Kadlec, J. Mater. Sci. 50 (2015) 6477–6490.
[45] Y. Bin, M. Mine, A. Koganemaru, X. Jiangand, M. Matsuo, Polymer 47 (2006) 1308–1317.
[46] M. Ren, F. Frimmeland, G. Abbt-Braun, J. Mol. Catal. A-Chem. 400 (2015) 42–48.